Leaky CPW-Based Slot Antenna Arrays for Millimeter-Wave Applications

Anthony Grbic, *Student Member, IEEE*, and George V. Eleftheriades, *Member, IEEE*

***Abstract*—A uniplanar leaky-wave antenna (LWA) suitable for operation at millimeter-wave frequencies is introduced. Both unidirectional and bidirectional versions of the antenna are presented. The proposed structure consists of a coplanar waveguide fed linear array of closely spaced capacitive transverse slots. This configuration results in a fast-wave structure in which the $n = 0$ spatial harmonic radiates in the forward direction. Since the distance, d, between adjacent elements of the array is small $d \ll \lambda_o$, the slot array essentially becomes a uniform LWA. A comprehensive transmission line model is developed based upon the theory of truncated periodic transmission lines to explain the operation of the antenna and provide a tool for its design. Measured and simulated radiation patterns, directivity, gain, and an associated loss budget are presented for a 32-element antenna operating at 30 GHz. The uniplanar nature of the structure makes the antenna appropriate for integration of shunt variable capacitors such as diode or micro-electromechanical system varactors for fixed frequency beam steering at low-bias voltages.**

***Index Terms*—Beam scanning, coplanar waveguide (CPW), integrated-circuit antennas, leaky-wave antennas (LWAs), millimeter-waves, slots.**

I. Introduction

RECENTLY, *printed* leaky-wave antennas (LWAs) have attracted much attention due to their high directivity, broad VSWR bandwidth performance, and frequency scanning capabilities. Antennas with dielectric and metal gratings have been studied extensively in the past and have attracted renewed inquiry [1]–[3]. In particular, there has been significant interest in the microstrip LWA, which utilizes a higher order radiative microstrip mode [4]–[8]. Since Menzel [9] first reported this leaky-wave structure, which was subsequently investigated by Oliner [10], many microstrip leaky-wave antenna designs incorporating various modifications have been explored. The microstrip LWA, however, has some notable drawbacks which include the requirement of special feeds to guard against the excitation of the dominant (slow-wave) microstrip mode [9], [11], [12]. In addition, the integration of shunt elements for beam steering at a fixed frequency becomes problematic in microstrip technology, especially at millimeter-wave frequencies, due to the need for via holes through the substrate [13]. On the other hand, the alternative solution of integrating series devices with the microstrip LWA can lead to prohibitively high control voltages [8].

Although, much work has been reported on printed LWAs at microwave frequencies, very little information can be found in literature on printed LWAs at millimeter-wave frequencies [1], [3], [7]. In fact, such antennas are particularly appealing at these frequencies since they become physically short while still providing high gain. Another salient feature of these antennas is that they employ a single series feed which results in reduced spurious radiation and conductor losses when compared to arrays fed by lossy and bulky corporate fed networks. This is particularly appealing at millimeter-wave frequencies where conductor losses increase dramatically. At the same time, a wide VSWR bandwidth can be achieved as opposed to series fed resonant antennas, which are notoriously narrowband in this regard.

Manuscript received June 6, 2001; revised September 20, 2001.

The authors are with the Edward S. Rogers Sr. Department of Electrical and Computer Engineering, University of Toronto, Toronto, ON M5S 3G4, Canada.

Digital Object Identifier 10.1109/TAP.2002.804259

II. Proposed Structure

A. Geometrical Layout

The proposed leaky-wave structure is shown in Fig. 1. As shown, the antenna is essentially a coplanar waveguide (CPW) transmission line loaded with radiative, transverse, series slots. Unlike the microstrip LWA, which exploits the *continuous* leakage of the (fast) first higher order TE mode, this structure belongs to the family of periodically loaded traveling-wave structures [14]. It is a basically fast-wave structure with a periodicity of $d \approx \lambda_o/5$. Due to this small axial period, the slot array can be thought of as essentially a *uniform* leaky-wave antenna [14]. A distinction should be made between this antenna and slow-wave periodically loaded structures such as dielectric grating antennas or image guide fed arrays [1], [15], [16]. In contrast to slow-wave structures which have a bound $n = 0$ spatial harmonic and radiate the $n = -1$ harmonic toward the backfire direction, this proposed structure is basically fast and radiates the $n = 0$ spatial harmonic toward the forward direction. Much like the Honey array (inductive grid), the proposed structure is a fast-wave radiating structure with periodicity $d \ll \lambda_o$ that supports leaky waves which radiate [14]. However, unlike the Honey array which has an inductive surface impedance that excites TE leaky-waves, the proposed array has a capacitive impedance which supports radiating TM leaky waves.

Since this new structure is entirely planar and CPW based, it offers several distinct advantages at millimeter-wave frequencies. Compared to the microstrip LWA, the proposed structure features a simple feed and the convenience of incorporating shunt devices without the need for via-holes and features a simple feed. This latter feature makes the structure appealing for periodic integration with shunt elements such as semiconductor varactors and micro-electromechanical system (MEMS) phase shifters [17] for fixed-frequency scanning along the longitudinal plane [8], [13]. With shunt integration of devices,

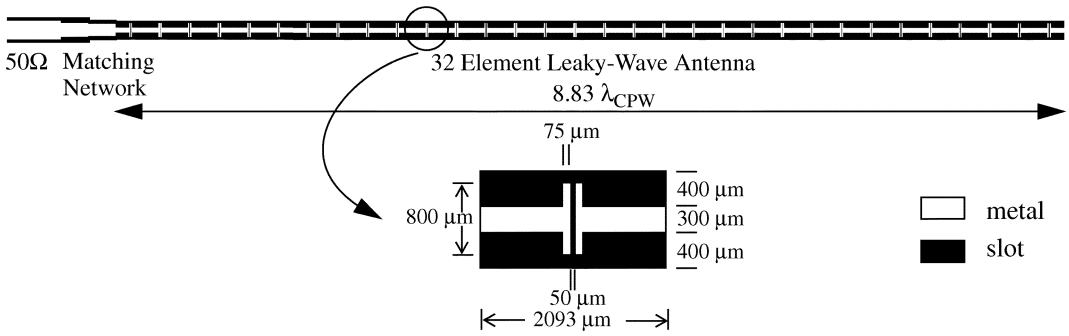

Fig. 1. Antenna configuration and dimensions at 30 GHz.

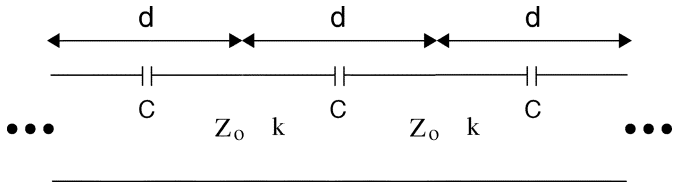

Fig. 2. Periodically loaded transmission line.

the corresponding control dc bias can be maintained at low levels. Most importantly, this antenna features a simple feed, unlike the feeds of the microstrip LWAs, which require special precautions to guard against the excitation of the dominant microstrip mode [8], [11], [18]. In addition, the transverse dimension of the proposed array is narrow. As a result, pencil beams could be formed in both principle planes by placing multiple LWAs in parallel, as has been demonstrated with microstrip LWA designs [5]. Likewise, low-cost, low-profile millimeter-wave switched beam arrays can be envisioned.

B. Principle of Operation

The LWA proposed in this paper, is axially periodic. The general Floquet-mode theory for periodically loaded LWAs is presented in [14]. In this section, however, the specific geometry of the proposed structure is examined based on a transmission line model describing the fundamental Floquet mode, with emphasis on the underlying physical mechanisms involved. Intuition into the properties of the antenna is gained through the study of ideal transmission lines, periodically loaded with series capacitances, as shown in Fig. 2. The ideal loaded transmission line system shown in Fig. 2 exhibits the following dispersion relation:

$$\cos(\beta d) = \cos(kd) + X \sin(kd)/2Z_o \tag{1}$$

where kd = phase delay of interconnecting transmission line segments, Z_o = characteristic impedance of interconnecting transmission line segments, βd = phase delay per periodic unit cell, and $X = 1/(\omega C)$ is the reactance due to the series loading capacitor. This dispersion relation can be examined graphically by means of the Brillouin diagram, shown in Fig. 3 for representative line and capacitive loading parameters. As expected, this diagram corresponds to a high-pass structure since the large reactance of the series capacitors impede propagation at low frequencies. Furthermore, the stopands are characterized by the cutoff condition $\beta d = n\pi$ where n is an integer. A simple trigonometric manipulation of (1) indicates that the bottom of

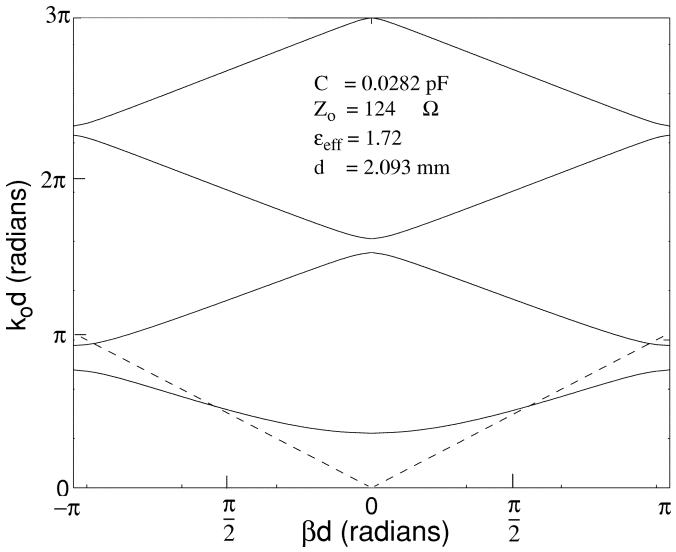

Fig. 3. k_o–β Brillouin diagram.

the first passband ($\beta d = 0$) is defined by a cutoff frequency given by

$$(kd)_c = \arctan\left(\frac{2q}{1-q^2}\right) \tag{2}$$

where $q = (X/(2Zo))$. On the other hand, at the bandpass edges where $\beta d = \pm\pi$, the dispersion relation of (1) implies that the propagation constants of the intrinsic and loaded lines become equal

$$\beta d = kd = \pm\pi \tag{3}$$

which is the well-known Bragg condition. It is apparent from Fig. 3, that the relative size of the bandgap becomes narrower with increased frequency. This is to be expected since the capacitive series reactance diminishes with increasing frequency, and the behavior of the structure approaches that of the intrinsic unloaded transmission line of characteristic impedance Z_o and propagation constant k. The dotted line in the Brillouin diagram of Fig. 3 marks the transition between slow and fast-wave propagation relative to free space ($k_o = \beta$) in the first Brillouin zone. As shown, for sufficiently small phase delays within the first passband, the corresponding periodic wave ($n = 0$ Floquet mode) becomes fast compared to free space (i.e., $\beta < k_o$) and the array becomes leaky.

An approximate, but very intuitive approach to understanding the propagation characteristics of the antenna structure, is to examine a relevant limiting case. Consider (2) for the special case of $X \ll Zo$ with the additional simplifying assumption that the interconnecting lines are short, i.e., $kd \ll 1$. In this case, the interconnecting lines can be modeled as inductances Ld, where L is the per-unit length inductance of the unloaded transmission line. These inductances appear in series with the loading capacitive reactances X. This simple model suggests that at cutoff, the reactance X cancels out the inductance Ld, and the effective propagation constant β vanishes. In this case, a very simple manipulation of the dispersion relation of (1), for small arguments, immediately reveals the following approximate expression for β around the bottom of the passband:

$$\beta = k\sqrt{(1-(\omega_c/\omega)^2} \tag{4}$$

where the cutoff frequency is given by $\omega_c = 1/\sqrt{(L(Cd))}$. In essence, the series capacitors reduce the effect of the interconnecting series inductances Ld. This results in a reduction of the effective propagation constant β and establishes a fast-wave propagation compared to the unloaded line. Under the leaky mode of operation, the beam emerges at an angle θ_m from broadside according to the relation

$$\theta_m = \arcsin(\beta/k_o). \tag{5}$$

This relation represents the transverse phase matching condition between the propagation constant of the emerging beam $\overline{k_o}$ and the propagating periodic wave on the loaded transmission line $\overline{\beta}$.

III. Design of the Unit Cell

The design process is outlined in this section. A specific example is considered for an emerging beam at 45° from broadside, at an operating frequency of $f_o = 30$ GHz. The corresponding substrate is assumed to be a 254-μm-thick Rogers RO3003 laminate with a relative permittivity, ϵ_r of 3.0. The substrate is deliberately chosen electrically thin in order to avoid strong excitation of substrate modes. Inevitably, this leads to bidirectional patterns which may or may not be desirable depending on the specific application. In order to provide maximum design flexibility, a unidirectional version of the proposed LWA is discussed in Section V.

A. Choice of Interelement Spacing

The attenuation along the leaky-wave structure, owing to radiation, is not known at the early stages of the antenna design. However, it can be assumed that the leakage is gradual, and thus the attenuation constant is small. This is a desirable condition which corresponds to an effective illumination of all the elements in the array and, therefore, a narrow beam for an electrically long structure. Under this assumption, ordinary uniform linear array theory can be employed for the initial stages of the design. The element pattern of the array corresponds to the radiating capacitive slots which are transverse and, therefore, radiate with an electric field polarization lying along the array axis.

Simple criteria were adopted for choosing the interelement distance d. The interelement distance was chosen such that there is a far-field null along the endfire direction. This was done in order to reduce scattering from the substrate edges and produce cleaner patterns. Due to the electrically thin substrate used, the same condition results in a null for the coupled TM_o surface-wave power pattern along the endfire direction (for thin substrates $\beta_{\mathrm{TM}_o} \cong k_o$), further reducing scattering from the substrate edges. In addition, the interelement spacing, d, was selected to achieve a 45° angle of emergence for attainable capacitive slot widths which were practically limited to 50 μm by the photolithographic etching facilities available to the authors. This yielded an interelement spacing $d = 2.093$ mm at 30 GHz.

B. Choice of Feed-Line Characteristic Impedance Z_o

As previously explained, the series capacitive loading decreases the effective inductance of the loaded line and therefore, also reduces the effective characteristic impedance (Bloch Impedance). The exact expression of the Bloch Impedance of the loaded line shown in Fig. 2 is given by

$$Z_B^{\pm} = \frac{\pm Z_o\left(\sin(kd) - \frac{X}{Z_o}\cos^2\left(\frac{kd}{2}\right)\right)}{\sqrt{1-\left(\cos(kd) - \frac{X\sin(kd)}{2Z_o}\right)^2}}. \tag{6}$$

The ratio X/Z_o is fixed by the dispersion relation once the angle of emergence is selected. Therefore, it is obvious from (6), that the Bloch impedance rises as the feed-line characteristic impedance Z_o is increased. In Section II, it was established that the loading capacitors decrease the series inductance of the interconnecting lines. Consequently, in order to maintain a reasonable Bloch impedance level in the range of 50 Ω, a high unloaded characteristic impedance $Z_o = 124\ \Omega$ was selected. The 124 Ω CPW interconnecting line has been chosen with a central conductor strip width of 300 μm and a gap width of 400 μm (see Fig. 1). It is perhaps interesting to point out that one of the benefits of using a CPW medium is highlighted by the need to realize such high characteristic impedances on an electrically thin substrate at 30 GHz. Indeed, a corresponding microstrip realization would result in relatively narrow lines (75 μm), which according to HP-Linecalc result in a per unit length attenuation loss (decibles per wavelength) that is 1.7 times higher than that of the chosen CPW line.

C. Final Unit Cell Layout

Now that the phase constant β, characteristic impedance of the unloaded line Z_o and interelement spacing d have been chosen, the required capacitive loading can be calculated from the dispersion relation of (1). The required reactance was found to be $X = 188\ \Omega$. This reactance translates into a required loading capacitances of $C = 0.0282$ pF per slot at 30 GHz.

As was observed in [2] for parallel-plate waveguide fed slots, the angle of emergence in a LWA is almost independent of the total number of slots. This implies that the phase constant is also approximately independent of the total number of slots. Therefore, an approximate method based on the use of a single unit cell in isolation was adopted to determine the required slot dimensions for achieving the desired loading capacitance C for a beam pointing direction of 45° at 30 GHz. For this purpose, HP-momentum was used to extract an equivalent circuit of a

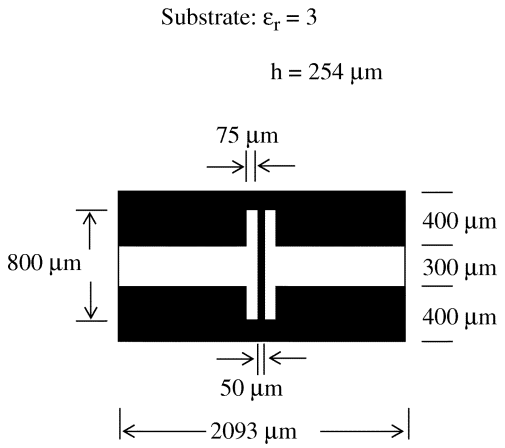

Fig. 4. Unit cell dimensions at 30 GHz.

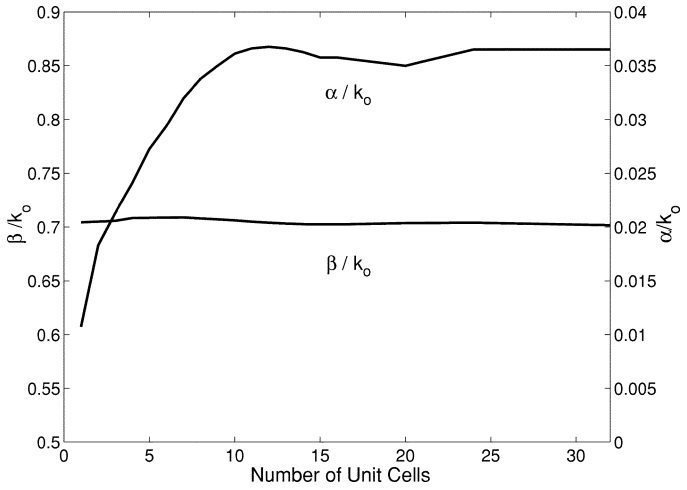

Fig. 5. Complex propagation constant versus number of unit cells in array.

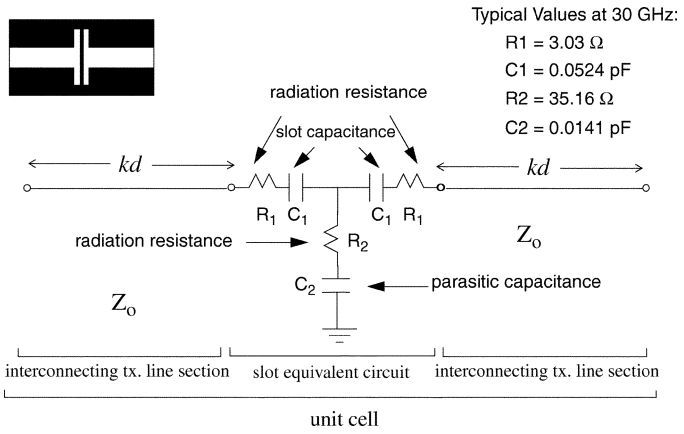

Fig. 6. Equivalent circuit for unit cell in array environment.

unit cell in isolation and optimize the geometrical parameters to achieve the required loading capacitance C. The determined unit cell dimensions are shown in Fig. 4. The exact equivalent circuit for the isolated unit cell is not shown here for brevity. In the next section, however, a similar equivalent circuit for the unit cell embedded in an infinite periodic environment is explicitly shown.

IV. Extraction of a Transmission Line Model and Corresponding Analysis

In this section, analysis techniques for truncated periodic structures are applied to the proposed structure of Fig. 1 and a useful transmission line model is extracted. The transmission line model is utilized for finalizing the LWA array design, including the selection of the number of unit cells N and the corresponding analysis of the far-field patterns and VSWR input impedance characteristics.

A. Extraction of a Transmission-Line Model for the Periodic Unit Cell

The analysis of a single isolated unit cell is inadequate for the determination of the leakage constant α of the antenna, due to mutual coupling and edge effects. However, for larger arrays of unit cells, edge effects become less significant and the propagation constant β, attenuation constant α, and Bloch impedance Z_B, approach that of an infinite array. In other words, the majority of the slots experience the same electromagnetic environment and therefore, it becomes quite reasonable to model the slots with identical equivalent circuits. The transmission-line equivalent circuit for the periodic unit cell was extracted from the propagation characteristics (propagation constant, attenuation and Bloch impedance) of entire arrays with various numbers of cells. Specifically, the propagation characteristics were computed from the two-port network representation of an N-element array obtained from HP-momentum simulations at the design frequency of 30 GHz. The results are described in Fig. 5, which shows the propagation constant and attenuation constant as a function of the number of unit cells in the array (up to $N = 32$). As shown in Fig. 5, the propagation constant, β, converges very quickly with increasing number of cells. This verifies the assumption that β can indeed be predicted based solely on a single isolated unit cell. On the other hand, the attenuation (leakage) constant converges for a much larger number of unit cells. For this particular geometry, more than 15 elements were required to achieve convergence.

Fig. 5 was utilized to determine the required number of unit cells, N, for the overall LWA. The length was chosen such that 95% of the incident power is radiated prior to reaching the antenna termination. Given that $\alpha = 0.048$ for larger arrays according to Fig. 5, the needed number of elements was found to be $N = 32$.

Once the number of cells was determined, the two-port characteristics of the entire 32-element array were utilized to extract the ABCD parameters of the embedded periodic unit cell based on simple transmission theory of cascaded two-ports. From these ABCD parameters of the periodic unit cell, the corresponding two-port equivalent transmission line circuit was extracted as shown in Fig. 6. The transmission lines to the left and to the right of the slot equivalent circuit represent the interconnecting CPW lines. Furthermore, the slot rcapacitance is represented by the series branch capacitors C_1, which are responsible for increasing the phase velocity of the periodic structure. On the other hand, the smaller shunt capacitance C_2 represents the parasitic capacitance between the slot plates and the CPW ground plane, which tends to slow down the periodic

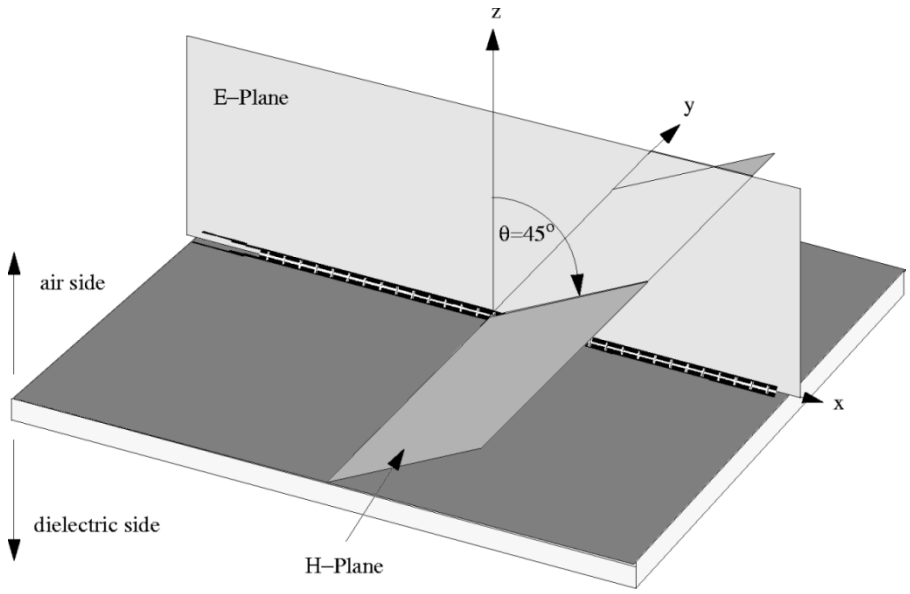

Fig. 7. Principle planes of the proposed antenna structure.

wave. Finally, the radiation (leakage constant) is represented by both the series and shunt resistance R_1 and R_2. It is perhaps worth noting that this equivalent circuit differs from that of an isolated unit cell predominantly in terms of the resistive components.

B. Analysis of Radiation Characteristics Based on the Transmission Line Model

The developed transmission line model has been utilized to quickly predict the radiation characteristics of the designed 32-element leaky-wave array. The far-field patterns were generated from slot excitations predicted using the developed transmission-line equivalent circuit.

From these slot currents, the far-field patterns were generated using the ordinary array factor

$$\text{Array Factor} = \sum_{n=1}^{32} I_n e^{j(n-1)k_o d \sin\theta} \tag{7}$$

where I_n is the current at the nth unit cell as predicted by transmission line theory and $(n-1)k_o d\sin\theta$ is the spatial progressive phase shift for an observation angle θ. With this array factor, an element factor corresponding to a slot antenna printed on a dielectric substrate was employed as determined by spectral-domain analysis techniques [19]. It is worth noting, that the simple transmission line model developed, based on the cascade of 32-unit cells (shown in Fig. 6) accounts for the fact that the structure is of finite length and is terminated in a short. Therefore, both forward and reverse traveling Bloch waves are represented in the model through standard theory of truncated periodic structures [20]. To facilitate the discussion of radiation patterns throughout the rest of this article, the principle radiation planes of the designed array are explicitly shown in Fig. 7. The corresponding E plane patterns at 30 GHz obtained from the transmission-line equivalent circuit are compared to the patterns from HP-momentum simulations in Fig. 8. As shown, there is excellent agreement between the two, validating

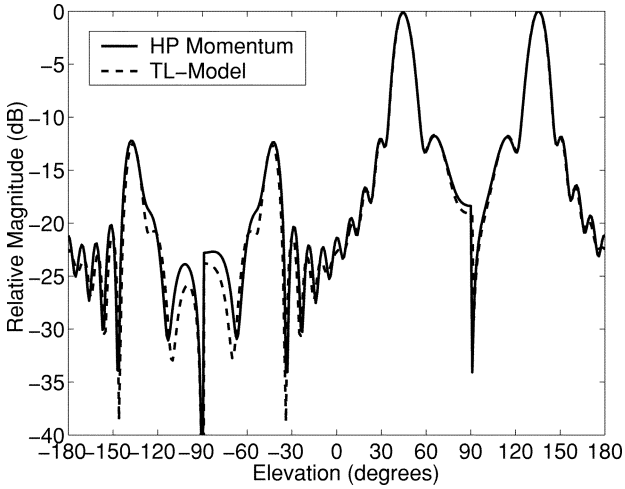

Fig. 8. E plane: HP-momentum versus TL-model.

the transmission-line model and providing a rapid vehicle for predicting the general radiation characteristics of the array. The mainlobe characteristics, as well as the level of the back lobe are accurately predicted. The slight discrepancies in the sidelobes can be ascribed to edge effects that are not accounted for by the transmission line model, since it consists of identical unit cells.

The computed propagation and attenuation constants are shown in Fig. 9 over a frequency range from 27 to 40 GHz based both on the transmission-line model and on direct HP-momentum simulations. First, note that the transmission-line model does a very good job in predicting the propagation constant β over a wide range of frequencies. The attenuation constant is also very well predicted, except in the slow-wave region where a residual attenuation of $\alpha/k_o \cong 0.03$ remains. As Fig. 9 shows, the dispersion relation exhibits high attenuation at low frequencies ($f < 28$ GHz) due to the increased series reactance of the capacitive slots. This corresponds to the stopband region of the lossless capacitively loaded transmission line case

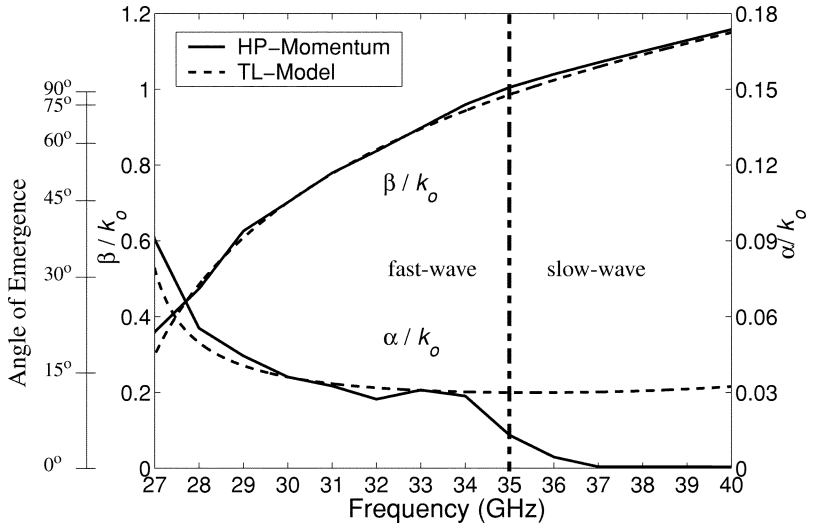

Fig. 9. Dispersion characteristic of CPW-based LWA.

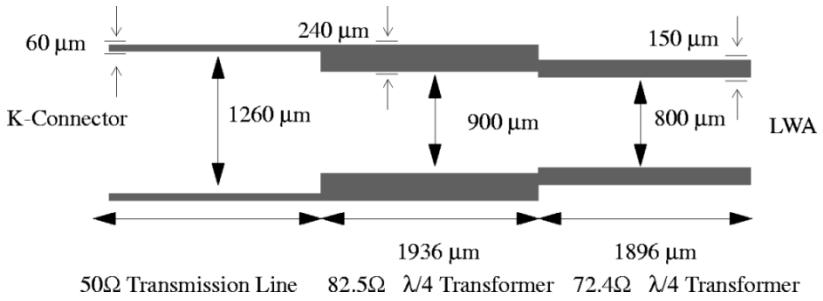

Fig. 10. Impedance matching network at antenna input.

shown in Fig. 3. Furthermore, the band edges are not as sharp as for the lossless capacitively loaded transmission line due to the presence of radiative losses modeled by the resistances R_1 and R_2, in Fig. 6. As the frequency is increased, a region of fast-wave propagation or leaky-wave operation is encountered. Further increase in frequency causes the phase delay of the interconnecting lines to increase and the series reactance of the capacitive slots to decrease. This leads to an increase of the propagation constant which translates to a beam tending toward the endfire direction with increasing frequency. Eventually, the antenna enters a region of slow-wave propagation when $\beta > k_o$ in compliance with the Brillouin diagram of Fig. 3.

V. Experimental Results

As mentioned in Section III, a Rogers RO3003 substrate with a relative permittivity 3.0 ± 0.04, a loss tangent of $\tan\delta = 0.000\,12$ and a half ounce copper metallization of 17 μm was used to fabricate the designed antenna at 30 GHz. Due to the symmetry of the structure shown in Fig. 1, it was decided not to use air-bridges along the array. This was deliberately done in order to demonstrate that excellent results can be achieved with a simple fabrication process. It should be noted that, according to simulation, the Bloch impedance of the loaded line at 30 GHz is about $40\ \Omega$ which was matched to the $50\ \Omega$ feed-line using a simple two-stage quarter-wavelength transformer as shown in Fig. 10. The antenna was fed through a flange-mounted K-connector launcher at the edge of the substrate and was terminated in a short as shown in Fig. 1.

A. Measured Far-Field Patterns

The E plane far-field patterns of the test antenna measured at 30 GHz, are shown in Fig. 11. As expected, the antenna radiates at an angle from broadside toward the direction of propagation. Furthermore, the measured maximum cross polarization in the E plane is reasonable at approximately -17.6 dB. Before the rest of the patterns are shown, the reader's attention should be drawn to the fact that the measured beam pointing direction is 55° and not 45° as was designed and predicted by the simulations of Fig. 8. A related discrepancy between the measured and narrower simulated beamwidth should also be pointed out. This issue was investigated extensively and it is believed that the observed discrepancies are due to the fact that the actual slots have a capacitance that is higher than what simulations predict. This increased capacitance can be attributed to the finite metallization of 17 μm, which cannot be easily modeled with a planar moment based solver such as HP-momentum. It can be argued, that this increased capacitance decreases the phase velocity on the periodic line, leading to the increased angle of emergence at 55° from broadside. To overcome the difficulty of simulating the structure with finite metallization using HP-momentum, the developed transmission line model came in very handy. Specifically, the capacitance, C_1, in the transmission-line model of

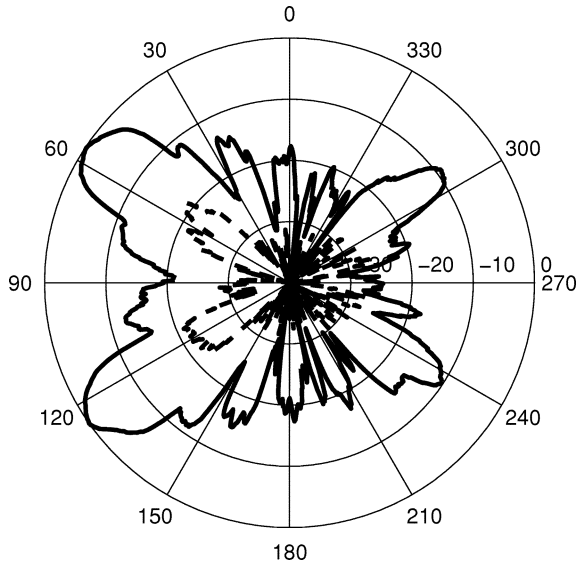

Fig. 11. Measured E plane pattern at 30 GHz.

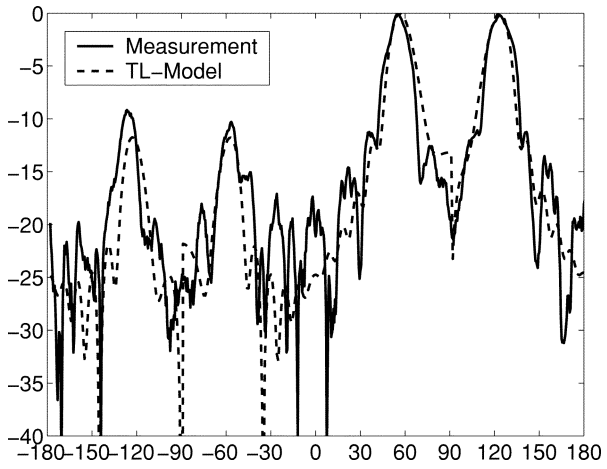

Fig. 12. E-plane: Modified transmission line model vs. experiment at 30 GHz.

Fig. 6 was increased from 0.0524 pF to 0.0592 pF, in order to steer the emerging beam from the designed direction to the measured one. The corresponding simulated E plane patterns are compared against the measured patterns in Fig. 12. As seen in this figure, this increase in capacitance also automatically recovers the experimental beamwidth and the two patterns now compare very well to each other. Therefore, it can be postulated that the increase in beamwidth is simply a result of scanning toward the endfire direction, as standard uniform (or slightly tapered) array theory for linear arrays would predict.

The corresponding measured air and dielectric side H plane patterns are shown in Fig. 13. The measured copolarization H plane patterns are compared against the patterns obtained from the modified transmission line model in Fig. 14. The highest cross-polarization levels are -12.3 dB and -10.8 dB on the air and dielectric sides, respectively. This higher cross polarization in the H plane, compared to the E plane, is predominantly due to the fact that in addition to the structure being fast wave, the CPW feedline also becomes fast, and thus, radiative. Along the longitudinal plane (XZ cut in Fig. 7), the far-field contributions of the two opposite magnetic currents of the CPW feedline exactly cancel out, thus leading to reduced cross-polarized fields in the E plane. However, this cancellation along the E plane creates two emerging cross-polarized beams in the H plane, on either side of the substrate which is apparent in Fig. 13.

B. Return Loss

The return loss of the antenna was measured from 24 to 36 GHz using a HP8722C vector network analyzer. The corresponding measurements are shown in Fig. 15 along with the simulated results obtained from the modified transmission line model. As shown, there is reasonable agreement between the measured and simulated results. Furthermore, Fig. 15 confirms that the VSWR performance of the antenna is quite broadband, although the beam-pointing direction changes with frequency. In this sense, the antenna can be considered broadband, in contrast to standard series fed resonant types of antennas, which exhibit a narrowband VSWR performance. Incidentally, this measured VSWR bandwidth, which corresponds to 26% for $|S_{11}| < -10$ dB is larger than the best corresponding bandwidth of 20% reported for the microstrip LWA [12]. This is due to the fact that the bandwidth of the latter is hindered by the special feeds needed to suppress the dominant microstrip mode. It should be noted, that in this present work the recorded 26% bandwidth does include the 50 Ω to 40 Ω two-stage quarter-wavelength transformer at the input of the array (see Fig. 10).

C. Loss Budget

A comprehensive loss budget is shown in Table I. The antenna directivity was estimated to be 11.3 dB by integrating the measured E and H plane far-field patterns using numerical integration. In order to evaluate the antenna radiation efficiency, the corresponding gain was also measured using the gain-transfer method and was found to be 9.2 dB.

In Table I, mismatch loss refers to the power lost due to reflections at the input terminals of the antenna. On the other hand, input line losses refer to the conductor and dielectric losses in the 50 Ω transmission line and the two-stage quarter-wavelength transformer (see Fig. 10). Furthermore, feed-line losses refer to the conductor and dielectric losses due to the CPW interconnecting lines of the unit cells along the array. Both the input line and feed-line losses were estimated using HP-Linecalc. For the case of the feed-line loss calculation, Linecalc was first used to estimate the attenuation loss per unit length of the raw CPW interconnecting line (i.e., assumed matched). Subsequently the transmission-line model of Section IV was utilized to account for the reverse wave reflected off the short-circuit termination of the array. The fact that this feed-line loss has been estimated to be only 0.4 dB is very encouraging and indicates that with proper design, there is no detrimental effect of the conductor losses to the performance of the array at 30 GHz. As Table I indicates there is a 0.8 dB loss unaccounted for. This discrepancy can be attributed to experimental errors which include 1) uncertainty in the measured absolute gain based on the gain transfer method [21], 2) error in estimating the directivity from the measured E and H plane patterns, and 3) errors in estimating conductor losses using HP-Linecalc. The 0.8 dB discrepancy falls

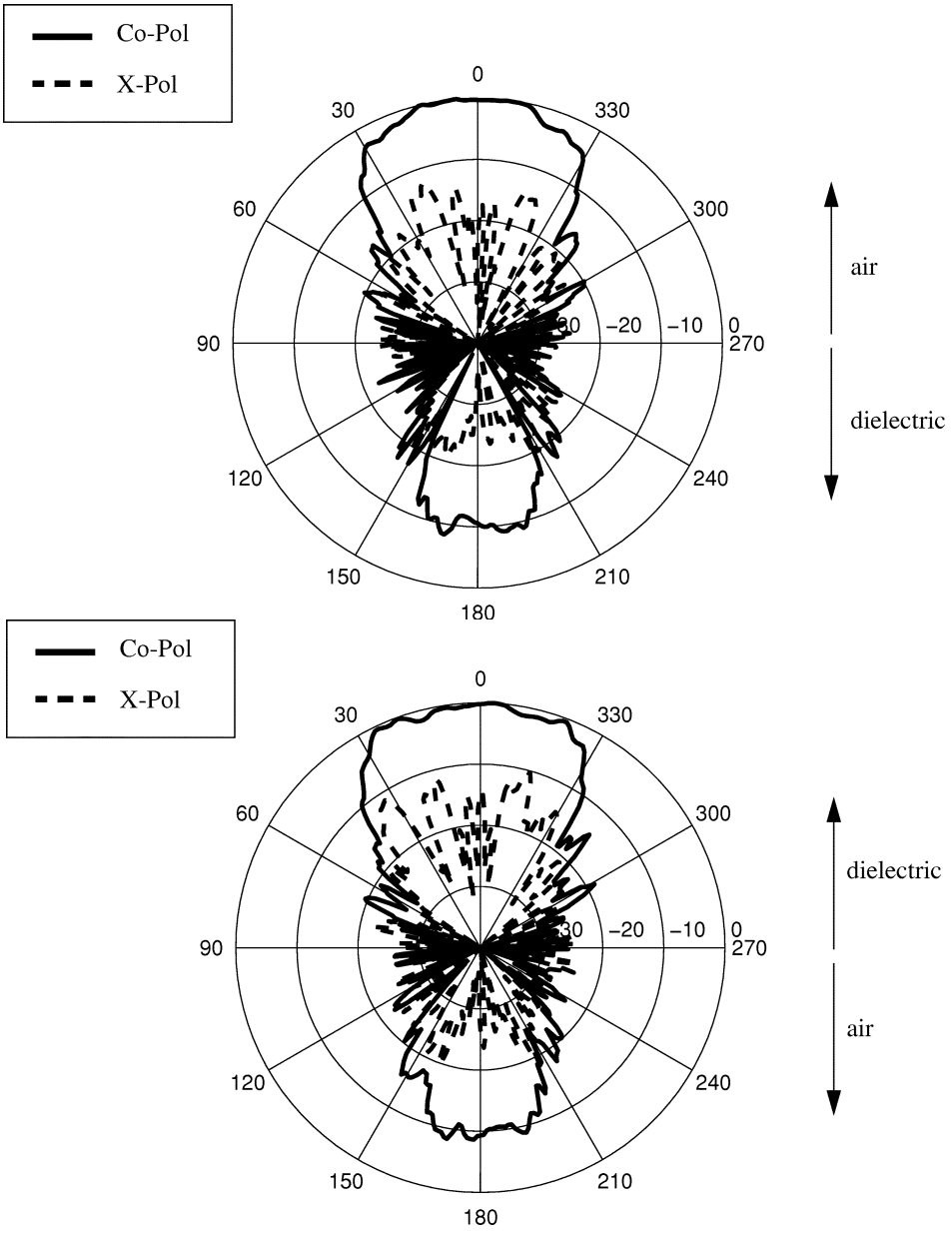

Fig. 13. Measured H plane patterns at 30 GHz.

within the cumulative error in estimating the directivity, gain, and feed-line losses reported in Table I.

D. Frequency Scanning Characteristics

As expected from the dispersion characteristic in Fig. 9, the main-beam scans as the operating frequency is swept. Within the antenna bandwidth (VSWR < 2), it was experimentally verified that the antenna scans from 21° (from broadside) at 25.5 GHz to 78° at 33.6 GHz. Furthermore, in the frequency range between 26–34 GHz, the measured gain variation is ± 1 dB from an average level of about 10 dB. An examination of the far-field patterns within this frequency range also reveals that there is a distinct pattern minimum at endfire ($\theta = 90°$) throughout most of this frequency range, despite the fact that an exact null was imposed only at 30 GHz.

E. Unidirectional Version of the Proposed LWA

For many applications it is preferred to employ unidirectional antennas. However, a slot antenna is essentially a bidirectional radiator. The standard way of suppressing the radiation from one side of a slot is to back it with a ground plane or a cavity. However, one must be careful because in the former case a parasitic TEM wave can be excited between the slot and backing ground planes, whereas in the latter case, spurious resonances can be introduced that limit the VSWR bandwidth. Recently, substantial progress has been made toward the realization of highly efficient unidirectional slot antennas and arrays. For example, excellent results have been achieved from ground plane backed linear slot arrays by suppressing the parasitic TEM mode using a phase cancellation technique [22]. Another effective method involves the use of an electromagnetic band-gap (EBG) material at the

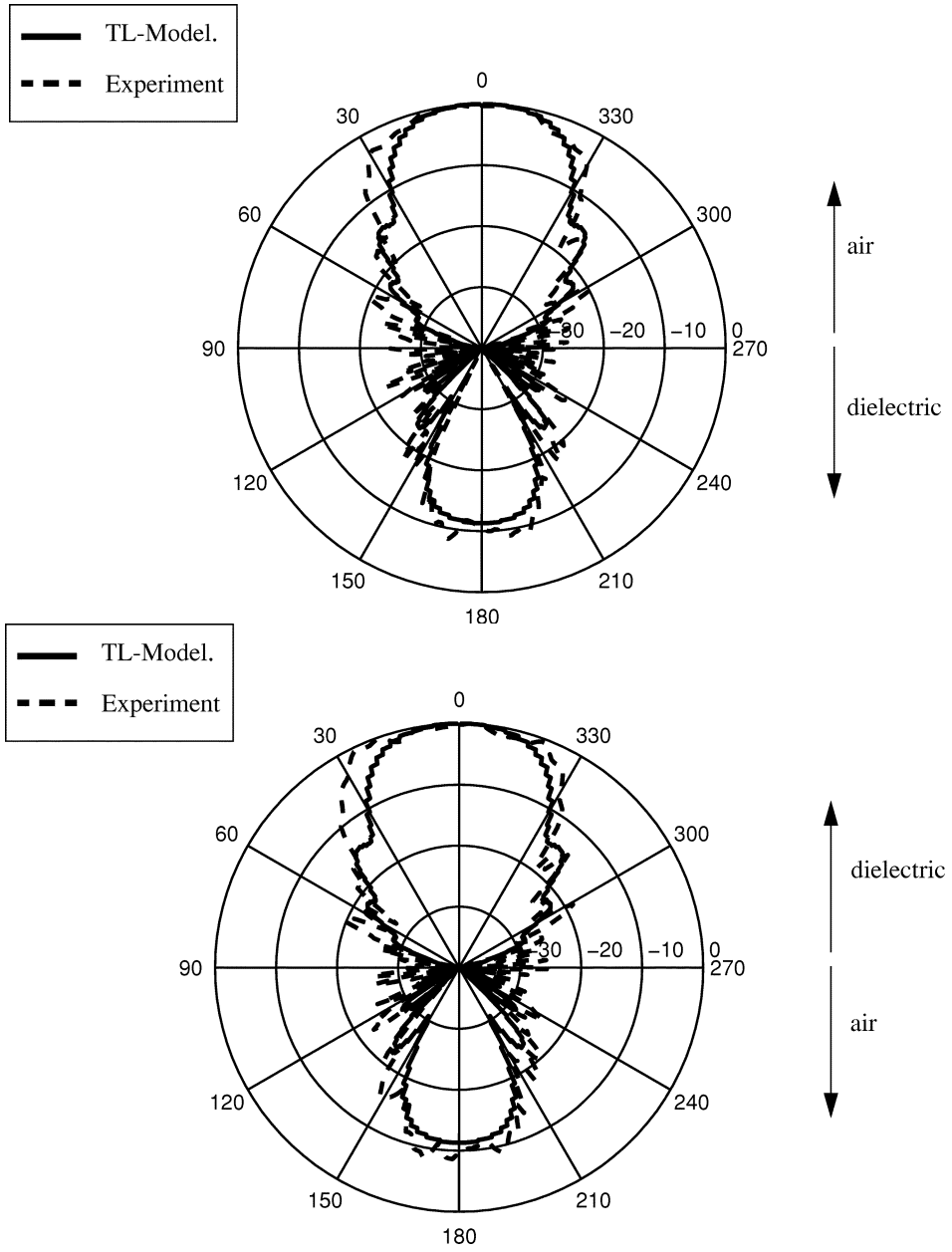

Fig. 14. H plane co-pol. patterns: Experiment versus transmission line model at 30 GHz.

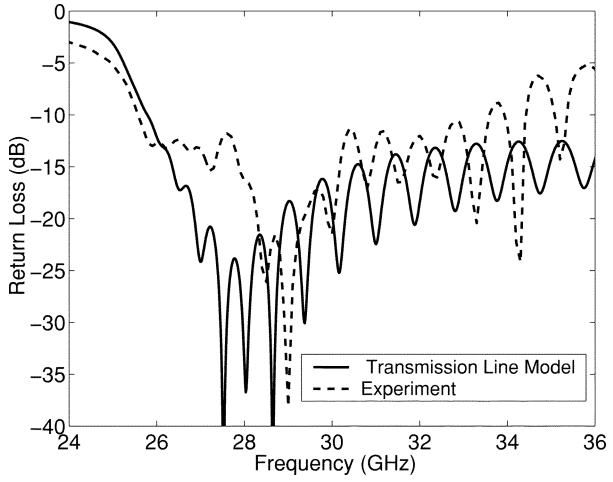

Fig. 15. Return loss: Experiment versus modified transmission line model.

back of the slot operating within its stopband to suppress the back radiation [24].

In order to render this proposed LWA antenna unidirectional, it was decided to exploit the feature that its transverse dimension is electrically short. This implies backing the LWA with a narrow, but long metallic trough, as shown in Fig. 16. The trough can be thought of as a waveguide operated well below the cutoff frequency of the dominant TE_{10} mode. This ensures that transverse resonances can be eliminated. Furthermore, since most of the power is radiated from the structure before it reaches the open end of the trough, any longitudinal resonances are eliminated. The corresponding measured E plane patterns at 30 GHz are shown in Fig. 17. As shown, this unidirectional version of the proposed LWA works exceptionally well, suppressing the back radiation below 20 dB. In addition, the measured return loss shown in Fig. 18 does not show any evidence of spurious

TABLE I
LOSS BUDGET

Directivity from Measured Patterns dB	11.3
Measured Gain dB	9.2
Mismatch Loss dB	0.1
Input Line Losses dB	0.8
Antenna Feed-line Losses dB	0.4
Unaccounted Losses dB	0.8

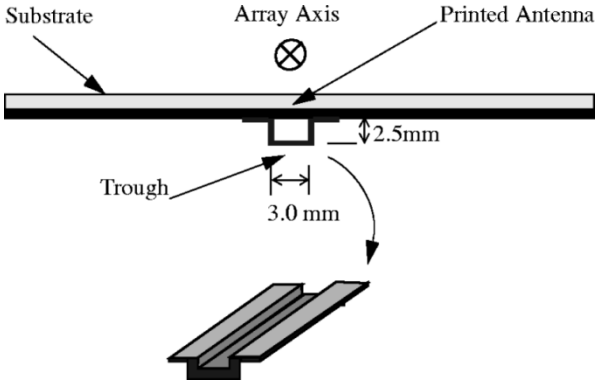

Fig. 16. Unidirectional design at 30 GHz.

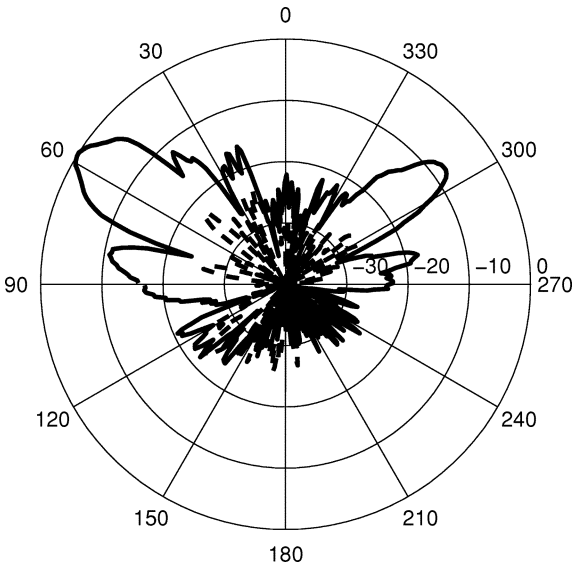

Fig. 17. Measured unidirectional E plane pattern at 30 GHz.

resonances appearing throughout the entire bandwidth or significant degradation. A 2-dB increase in the measured gain was observed for the unidirectional antenna over the bidirectional one, illustrating that most of the back radiation is recovered by the backing trough.

VI. CONCLUSION

A new uniplanar LWA operating at millimeter-wave frequencies has been introduced and both unidirectional and bidirectional versions of the antenna have been presented. This structure utilizes a capacitive surface of closely spaced slots that excites a fast $n = 0$ spatial harmonic, which radiates. Unlike the standard microstrip LWA, there is no need

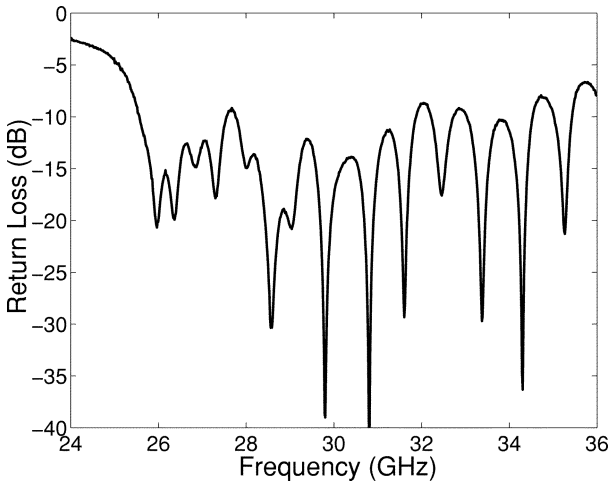

Fig. 18. Return loss for unidirectional design.

for special, mode suppression feeds, thus, rendering the proposed structure inherently broadband. Furthermore, the new antenna permits the simple integration of shunt phase control devices such as semiconductor or MEMS varactors for fixed frequency beam scanning applications. The shunt integration of devices would allow the dc control bias to be maintained at low levels. In addition, the transverse size of the structure is electrically narrow, which allows the compact integration of several antennas side-by-side in order to form pencil or switched beams.

A simple transmission-line model has been introduced to understand the operation of the new antenna and facilitate its design. Based on this model and refinements through method of moments electromagnetic simulations, a LWA has been designed at 30 GHz. The prototype antenna has been tested successfully and points at an angle of 55° from broadside while exhibiting a VSWR < 2 bandwidth of 26%. In addition, the antenna demonstrates a gain of 9.2 dB while suffering only minimal conductor feed-line losses of 0.4 dB.

Inspired by this present work, a backward radiating version of this leaky-wave antenna was subsequently reported by the authors in [24].

REFERENCES

[1] F. Schwering, "Millimeter wave antennas," *Proc. IEEE*, vol. 80, pp. 92–102, Jan. 1992.
[2] C. Lee and H. Son, "Periodically slotted dielectrically filled parallel-plate waveguide as a leaky-wave antenna: E-polarization case," *IEEE Trans. Antennas Propagat.*, vol. 47, pp. 171–178, Jan. 1999.
[3] T. Teshirogi, Y. Kawahara, A. Yamamoto, Y. Sekine, N. Baba, and M. Kobayashi, "High-efficiency, dielectric slab leaky-wave antennas," *IEICE Trans. Commun.*, vol. E84-B, pp. 2387–2394, Sept. 2001.
[4] C. Luxey and J.-M. Laheurte, "Simple design of dual-beam leaky-wave antennas in microstrips," *Proc. Inst. Elect. Eng.* , vol. 144, pp. 397–402, Dec. 1997.
[5] C.-N. Hu and C. Tzuang, "Microstrip leaky-mode antenna array," *IEEE Trans. Antennas Propagat.*, vol. 45, pp. 1698–1699, Nov. 1997.
[6] T.-L. Chen and Y.-D. Lin, "Microstrip leaky-wave antenna fed by short-end CPW-to-slot transition," *Electron. Lett.*, vol. 35, pp. 100–101, Jan. 1999.
[7] C. Lin and C. Tzuang, "A dual-beam micro-CPW leaky-mode antenna," *IEEE Trans. Antennas Propagat.*, vol. 48, pp. 310–316, Feb. 2000.
[8] K. Noujeim and K. Balmain (Chair), "Fixed-frequency beam-steerable leaky-wave antennas," Ph.D. dissertation, Dept. Elect. Comput. Eng., Univ. Toronto, Toronto, ON Canada, 1998.
[9] W. Menzel, "A new travelling-wave antenna in microstrip," *Arch. Elek. Ubertragung.*, vol. 33, pp. 137–140, Apr. 1979.

[10] A. Oliner and K. Lee, "Microstrip leaky wave strip antennas," in *Proc. IEEE Int. Antennas Propagat. Symp. Dig.*, Philadelphia, PA, June 1986, pp. 443–446.
[11] Y. Lin, J. Sheen, and C. Tzuang, "Analysis and design of feeding structures for microstrip leaky wave antenna," *IEEE Trans. Microwave Theory Tech.*, vol. 44, pp. 1540–1547, Sept. 1996.
[12] Y. Qian, B. Chang, T. Itoh, K. Chen, and C. Tzuang, "High efficiency and broadband excitation of leaky mode in microstrip structures," in *Proc. IEEE Microwave Theory Tech. Dig.*, vol. 4, Anaheim, CA, June 1999, pp. 1419–1422.
[13] J. James, G. Evans, and A. Fray, "Beam scanning microstrip arrays using diodes," *Proc. Inst. Elect. Eng. Microwaves, Antennas, Propagat.*, vol. 140, pp. 43–51, Feb. 1993.
[14] R. Collin and F. Zucker, *Antenna Theory, Part II*. New York: McGraw-Hill, 1969.
[15] T. Itoh, "Application of gratings in a dielectric waveguide for leaky-wave antennas and band-reject filters," *IEEE Trans. Microwave Theory Tech.*, vol. 25, pp. 1134–1138, Dec. 1977.
[16] C.-Y. Lee, A. Basu, J. S.-M. Wong, B. Houshmand, and T. Itoh, "Millimeter-wave dielectric leaky-wave antennas," in *Proc. URSI Int. Symp. Signals, Syst. Electron.*, San Francisco, CA, Oct. 1995, pp. 21–24.
[17] N. Barker and G. Rebeiz, "Distributed MEMS true-time delay phase shifters and wideband switches," *IEEE Trans. Microwave Theory Tech.*, vol. 46, pp. 1881–1890, Nov. 1998.
[18] W. Deal, Y. Qian, and T. Itoh, "Planar integrated antenna technology," *Microwave J.*, pp. 128–144, July 1999.
[19] C. Balanis, *Antenna Theory*. New York: Wiley, 1997.
[20] D. Pozar, *Microwave Engineering*. New York: Wiley, 1998.
[21] D. M. Pozar and B. Kaufman, "Comparison of three methods for the measurement of printed antenna efficiency," *IEEE Trans. Antennas Propagat.*, vol. 36, pp. 36–139, Jan. 1988.
[22] M. Qiu, M. Simcoe, and G. V. Eleftheriades, "High gain meanderless slot arrays on electrically thick substrates at mm-wave frequencies," *IEEE Trans. Microwave Theory Tech.*, vol. 50, pp. 517–528, Feb. 2002.
[23] J. Shumpert, W. Chappell, and L. Katehi, "Parallel-plate mode reduction in conductor-backed slots using electromagnetic bandgap substrates," *IEEE Trans. Microwave Theory Tech.*, vol. 47, pp. 2099–2104, Nov. 1999.
[24] A. Grbic and G. V. Eleftheriades, "Experimental verification of backward-wave radiation from a negative refractive index metamaterial," *J. Appl. Phsy.*, vol. 92, pp. 5930–5935, Nov. 2002.

Anthony Grbic (S'00) received the B.A.Sc. and M.A.Sc. degrees in electrical engineering from the University of Toronto, Toronto ON, Canada, in 1998 and 2001, respectively. He is currently working toward the Ph.D. degree at the same institution.

His research interests include planar millimeter-wave antennas, circuits, and periodic structures.

Mr. Grbic received the Best Student Paper Award, at the 2000 Antenna Technology and Applied Electromagnetics Symposium.

George V. Eleftheriades (S'86–M'88) received the Diploma degree in electrical engineering from the National Technical University of Athens, Athens, Greece, and the M.S.E.E. and Ph.D. degrees in electrical engineering from the University of Michigan, Ann Arbor, in 1988, 1989, and 1993, respectively.

From 1994 to 1997, he was with the Swiss Federal Institute of Technology, Lausanne, Switzerland, where he was engaged in the design of millimeter and submillimeter-wave receivers, and in the creation of fast CAD tools for planar packaged microwave circuits. Currently, he is an Assistant Professor, with the Department of Electrical and Computer Engineering, University of Toronto, Toronto, ON Canada. He is author or coauthor of more than 70 articles in refereed journals and conference proceedings.

Dr. Eleftheriades received the Gordon Slemon Teaching Award from the University of Toronto and the Ontario Premier Research Excellence Award in 2001. He was a corecipient of the Best Paper Award, 6th International Symposium on Antennas (JINA), France, 1990, he received a Student Paper Award in the 1992 IEEE Antennas and Propagation Symposium and the Distinguished Achievement Award from the University of Michigan, in1991.